AGU PUBLICATIONS

JGR

Journal of Geophysical Research: Atmospheres

RESEARCH ARTICLE

10.1002/2016JD026221

Key Points:
- Extractive electrospray ionization mass spectrometry can be used to assess reaction kinetics in oleic acid aerosols
- The most important sinks for Criegee intermediates formed during oleic acid ozonolysis are isomerization and secondary ozonide formation
- The Pretty Good Aerosol Model can reproduce measurements of evolving reactant loss, product formation, and particle size change

Supporting Information:
- Supporting Information S1

Correspondence to:
P. J. Gallimore and P. T. Griffiths,
pjg48@cam.ac.uk;
ptg21@cam.ac.uk

Citation:
Gallimore, P. J., P. T. Griffiths, F. D. Pope, J. P. Reid, and M. Kalberer (2017), Comprehensive modeling study of ozonolysis of oleic acid aerosol based on real-time, online measurements of aerosol composition, *J. Geophys. Res. Atmos.*, *122*, 4364–4377, doi:10.1002/2016JD026221.

Received 11 NOV 2016
Accepted 7 MAR 2017
Accepted article online 20 MAR 2017
Published online 18 APR 2017

Comprehensive modeling study of ozonolysis of oleic acid aerosol based on real-time, online measurements of aerosol composition

P. J. Gallimore[1], P. T. Griffiths[1,2], F. D. Pope[3], J. P. Reid[4], and M. Kalberer[1]

[1]Department of Chemistry, University of Cambridge, Cambridge, UK, [2]NCAS-Climate, Department of Chemistry, University of Cambridge, Cambridge, UK, [3]School of Geography, Earth and Environmental Sciences, University of Birmingham, Birmingham, UK, [4]School of Chemistry, University of Bristol, Bristol, UK

Abstract The chemical composition of organic aerosols profoundly influences their atmospheric properties, but a detailed understanding of heterogeneous and in-particle reactivity is lacking. We present here a combined experimental and modeling study of the ozonolysis of oleic acid particles. An online mass spectrometry (MS) method, Extractive Electrospray Ionization (EESI), is used to follow the composition of the aerosol at a molecular level in real time; relative changes in the concentrations of both reactants and products are determined during aerosol aging. The results show evidence for multiple non-first-order reactions involving stabilized Criegee intermediates, including the formation of secondary ozonides and other oligomers. Offline liquid chromatography MS is used to confirm the online MS assignment of the monomeric and dimeric products. We explain the observed EESI-MS chemical composition changes, and chemical and physical data from previous studies, using a process-based aerosol chemistry simulation, the Pretty Good Aerosol Model (PG-AM). In particular, we extend previous studies of reactant loss by demonstrating success in reproducing the time dependence of product formation and the evolving particle size. This advance requires a comprehensive chemical scheme coupled to the partitioning of semivolatile products; relevant reaction and evaporation parameters have been refined using our new measurements in combination with PG-AM.

1. Introduction

Organic compounds comprise a significant fraction of fine aerosol particle mass in the atmosphere [*Murphy et al.*, 2006]. The chemical composition of both directly emitted, primary organic particles and those formed by secondary processes is transformed continuously in the atmosphere [*Ziemann and Atkinson*, 2012], with contingent but poorly understood influences on the Earth's climate [*Boucher et al.*, 2013] and human health [*Pope et al.*, 2009].

Heterogeneous and in-particle reactions of organic compounds are particularly poorly understood. In-particle reactivity is complicated by the strong influence of composition (aerosol water content, ionic strength, organic functional group concentrations, etc.) on observed reactions and products [*Kroll and Seinfeld*, 2008]. In addition, identifying individual reaction pathways in chemically complex mixtures is a difficult analytical and conceptual challenge [*Noziere et al.*, 2015]. Previous studies have attempted to quantify reactive uptake to particles [*Liggio and Li*, 2006; *Rudich et al.*, 2007] and lifetimes of marker compounds in aerosols with respect to heterogeneous oxidation [*Robinson et al.*, 2007; *Zhao et al.*, 2014]. The thermodynamic viability of some reversible accretion reactions in particles has also been assessed [*Barsanti and Pankow*, 2005, 2006]. In general, however, there is a need for detailed studies which elucidate the major products, channels, and pathways of in-particle reactions as a starting point for assessing their atmospheric implications.

This study presents a combined measurement and modeling approach to understand product formation mechanisms and kinetics during the heterogeneous ozonolysis of oleic acid (OA) particles. Oleic acid is a low vapor pressure unsaturated fatty acid. Fatty acids are an important class of compounds in the atmosphere [*Rogge et al.*, 1993; *Mochida et al.*, 2002; *Wang et al.*, 2006], and moreover, OA aerosols have become an important test case for our understanding of heterogeneous and in-particle reactions [*Ziemann*, 2005; *Zahardis and Petrucci*, 2007]. Here time-resolved molecular composition measurements are obtained from a recently developed mass spectrometry (MS) technique, Extractive Electrospray Ionization (EESI) [*Gallimore and Kalberer*, 2013]. EESI-MS is an online method capable of extracting and ionizing organic analytes from

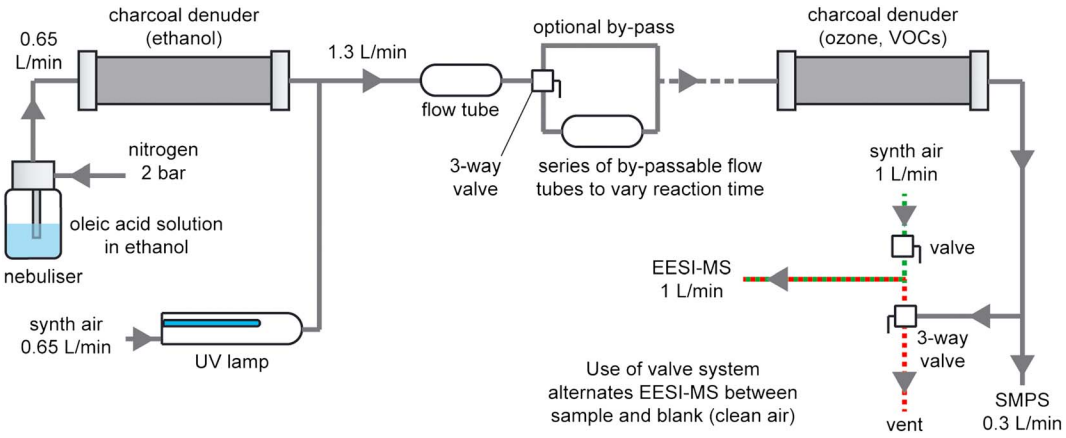

Figure 1. Schematic diagram of laboratory setup for ozonolysis of oleic acid aerosol and chemical characterization. The ozone and aerosol were rapidly mixed so the exposure time was defined by the variable reaction volume between mixing and the second denuder. The steady state aerosol composition for a particular ozone exposure was acquired using EESI-MS, and the ion source was flushed with clean air between samples and "blank" spectra were recorded during this time.

aerosols to produce molecular ions with minimal fragmentation. Intensity changes of reactant and product ions can be related to concentration changes in particles.

A few explicit or near-explicit models of organic aerosol chemistry have been described in recent years [*Griffiths et al*., 2009; *McNeill et al*., 2012; *Berkemeier et al*., 2013; *Houle et al*., 2015]. These provide a flexible and rigorous framework in which to test our understanding of aerosol chemistry and transport phenomena, in so far as relevant physicochemical data are available. Comparison with detailed measurements is essential for model validation; their predictive ability can then be used to probe experimentally inaccessible phenomena, refine uncertain parameters, and provide a link between experiment and larger-scale models. Here we use the Pretty Good Aerosol Model (PG-AM) adapted from *Griffiths et al*. [2009]. Reaction, diffusion, and interfacial transport are represented explicitly in the model based on evaluated physical parameters derived from the literature. We compare to a range of previous observations of oleic acid loss and particle size change. We have also built a detailed chemical mechanism to capture the time dependence of multigenerational product formation observed by EESI-MS, in particular elucidate the fates of Criegee intermediates (CIs) formed during ozonolysis.

2. Methods

2.1. Aerosol Flow Tube Experiments

Oleic acid particles were generated in the laboratory and reacted with ozone according to the scheme in Figure 1. A solution of 3 mmol/L oleic acid (99%, Sigma Aldrich) in ethanol (analytical reagent grade, Fisher) was prepared for use in a custom-built constant-output nebulizer. The nebulizer was supplied with nitrogen (oxygen free, BOC) at a pressure of 2 bar and output flow rate of 0.65 L/min. A charcoal denuder was employed to remove ethanol from the particles, although small amounts (we estimate a few percent on a molar basis) were detected in the MS analysis. No water was added to the system, and the measured relative humidity was less than 5% throughout the experiments. Ozone was produced by flowing synthetic air (zero grade, BOC) through a photolysis tube containing a mercury UV lamp (Pen-Ray 3SC-9, UVP) at 0.65 L/min. The concentration of ozone was varied by partially covering the lamp with an aluminum sheath. It was varied between 8 and 22 ppm, determined after mixing with the aerosol flow using a UV photometric ozone analyser (Thermo Scientific model 49i). Experiments were performed in an air-conditioned laboratory at 20°C.

A series of steady state reaction times between oleic acid particles and ozone were established using five by-passable flow tubes. The aerosol and ozone were mixed into a 4 mm inner diameter Teflon tube. The Reynolds number (*Re*) of the fluid flow was calculated as *Re* ~110, and a laminar mixing time < 0.1 s was therefore estimated based on *Keyser* [1984]. The reaction time was estimated by dividing the total reaction volume by the volumetric flow rate. The total reaction volume could be varied between 0.1 and 5.4 L resulting in reaction times of ~3–140 s. A second charcoal denuder was employed after the reaction volumes to

remove any remaining ozone and gas-phase organic species. The polydisperse aerosol size distribution was monitored using a scanning mobility particle sizer (TSI model 3936). A single mode was observed with a geometric standard deviation of 1.8 and a typical particle mass loading of 5 mg/m^3. To account for the full aerosol volume and surface area distributions, an "effective" average particle radius, $r_{eff} = 3V_t/S_t$, was calculated [*Stewart et al.*, 2004]. For fresh particles, r_{eff} was determined to be 250 nm and was used as the particle radius in the model simulations described below.

2.2. EESI-MS Operation

The EESI source is described in detail by *Gallimore and Kalberer* [2013]. Briefly, it consists of a custom-built aerosol injector and housing which is interfaced with a commercially available electrospray ionization source (Thermo Scientific HESI-II). The primary solvent electrospray was a water-methanol 1:1 mixture (Optima LC-MS grade solvents, Fisher Scientific) containing 0.05% formic acid (90%, Breckland Scientific) and was operated in negative ionization mode with a spray voltage of −3.0 kV. The aerosol injector delivered particles at a flow rate of 1 L/min into the primary solvent spray. Particle-droplet collisions dissolve the aerosol analytes, which are ionized and ejected into the gas phase by a Coulomb explosion mechanism typical for electrospray ionization.

The EESI-MS acquisition was varied between blank and sample measurements from the aerosol flow tube setup. Prior to blank measurements, air was flushed through the source for 15 min to remove particles from the previous sample while the aerosol flow was diverted to a vent. During sample measurements, the flushing air flow was switched off and the aerosol diverted into the EESI source. This assured a constant flow of 1 L/min into the source was maintained at all times. Mass spectrometry measurements were made using an ultrahigh-resolution mass spectrometer (Thermo Scientific LTQ Orbitrap Velos). The high mass accuracy (<2 ppm) and resolution ($m/\Delta m$ = 100 000 at m/z 400) of this instrument mean that unambiguous molecular formula assignments for reaction product ions are usually achieved.

Measurements were repeated 3 times for each reaction time, and the standard deviation of the relative peak intensities in the mass spectra were calculated (uncertainty on the ordinate in kinetic plots). The largest uncertainty related to ozone exposure (abscissa in kinetic plots) was the observation of limited quantities of oleic acid oxidation products (5–7%) even before deliberate ozone exposure. This prior exposure (for example, in the nebulizer or during sample preparation) was estimated by extrapolating best fit curves of the major products (azaleic acid (AA), 9-oxononanoic acid (9-ON), and nonanoic acid (NA)) back to a hypothetical "zero" intensity where they intercepted the ozone exposure axis. A prior exposure of 1.6×10^{-5} atm s was estimated and used in Figures 4 and 5.

2.3. Numerical Simulation of Aerosol Processes

In support of the measurements, we compared the results against a numerical model of reactive uptake of ozone by oleic acid aerosol. The Pretty Good Aerosol Model (PG-AM) describes the coupled uptake and evaporation to the gas phase, as well as coupled reaction/diffusion processes occurring within the aerosol.

The approach is based on the work by *Griffiths et al.* [2009] used in the study of reactive uptake of N_2O_5, in which the aerosol particle is treated as a series of concentric equal-volume shells, and uptake is modeled as a series of coupled reaction-diffusion equations. For this work, diffusion is parameterized as in *Griffiths et al.* [2009] and the reactions treated by the coupled equations were modified to include a mechanism for oleic acid ozonolysis including higher-order reactions between products, as described in section 2.4. The model is based as far as possible on a physically based description of the chemistry and transport and uses as input experimentally accessible parameters such as diffusion coefficients and solubilities. Table S1 gives the parameters employed here.

The model is written in Mathematica v10 (Wolfram) and the equations integrated forward in time using the NDSolve routine. For this work, uptake to a single representative aerosol particle was studied. The radius was set to the effective radius of the measured aerosol distribution ($r_{eff} = 3V_t/S_t$) and the time dependence of aerosol components simulated for an initial pure oleic acid particle on exposure to the measured ozone field. When comparing with our experiments, a degree of uncertainty may be introduced by size-dependent uptake from a polydisperse aerosol ensemble.

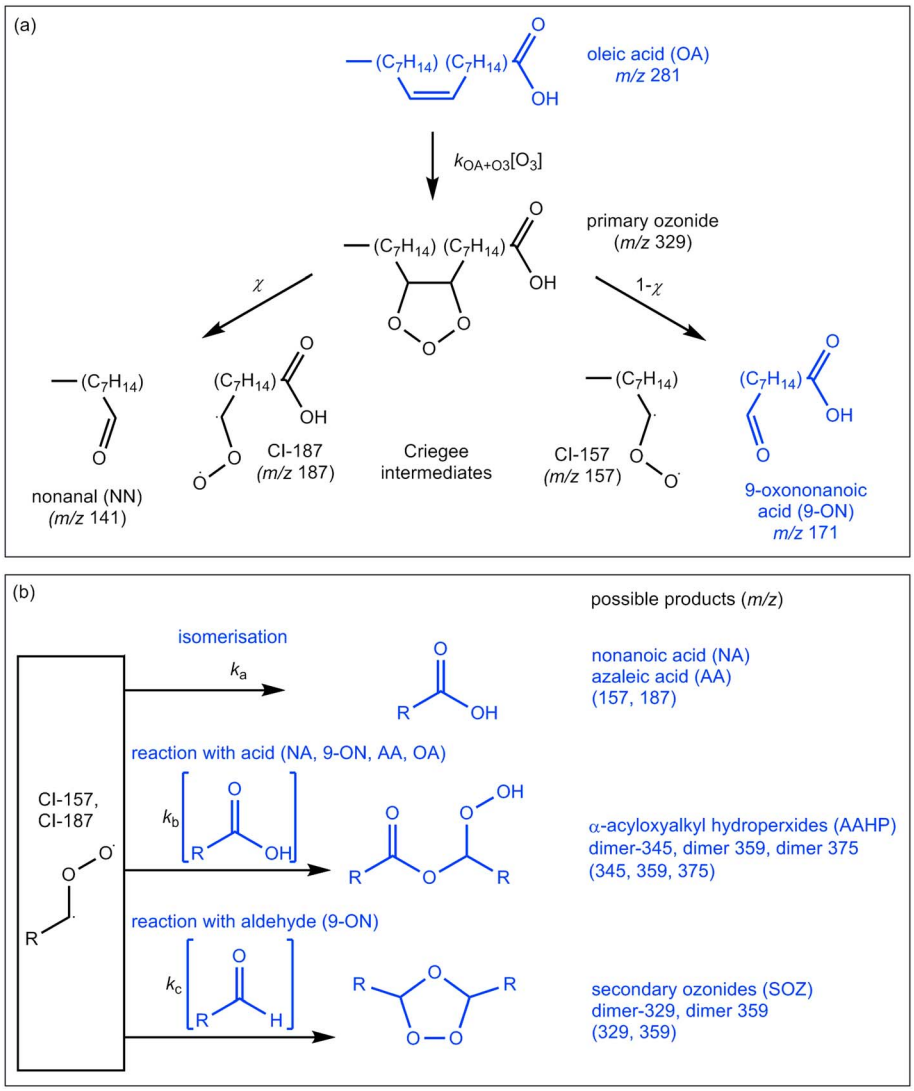

Figure 2. Chemical mechanism of oleic acid ozonolysis implemented in the model. (a) Primary C_9 products and Criegee intermediates formed from the initial ozone-alkene cycloaddition. (b) Reactions of the Criegee intermediates: isomerization to form carboxylic acids (k_a) and reactions with other functional groups to form dimers (k_b and k_c). k_{OA+O3}, χ, and k_a were estimated from the literature; k_b and k_c were adjusted to achieve the best fit to the measurements. We assign structures in blue to observed *m/z* but assume the proposed black structures (intermediates and volatile products) would not be observed.

2.4. Model Mechanism for Ozonolysis of Oleic Acid Aerosol

The formation of low molecular weight C_9 products from oleic acid ozonolysis has been reviewed in the literature [*Ziemann*, 2005; *Zahardis and Petrucci*, 2007; *Lee et al.*, 2012] and is outlined in Figure 2a. The ozone-alkene cycloaddition produces a short-lived primary ozonide which decomposes into an aldehyde and a rapidly stabilized Criegee intermediate (CI). We assume CIs are stabilized in the subsequent discussion. Large nonanal (NN) yields have been observed in previous studies [*Vesna et al.*, 2009; *Wang et al.*, 2016] suggesting that the NN + CI-187 route is favored over the 9-oxononanoic acid (9-ON) + CI-157 route. Formation of nonanoic and azaleic acids (NA and AA) from CIs is often described as a pseudounimolecular isomerization [*Ziemann*, 2005] (k_a in Figure 2b) with a plausible mechanism proposed by *Zahardis et al.* [2005]. The model parameters k_{OA+O3}, χ, and k_a were estimated from the literature and are detailed in Table S1.

The products formed from secondary reactions depend critically on the fates of the CIs. A particular focus of our work is to better constrain the relative rates of these CI reactions. Although a large number of reactions

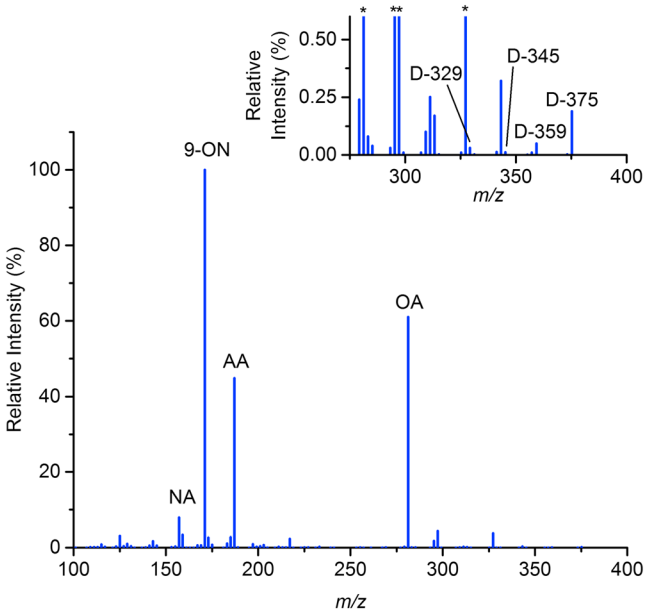

Figure 3. Mass spectrum of partially oxidized oleic acid aerosol acquired using EESI-MS. The initial particle-phase products of oleic acid ozonolysis, nonanoic acid (NA), 9-oxononanoic acid (9-ON), and azaleic acid (AA) are detected along with unreacted oleic acid (OA). The inset graph is an expansion of the region above *m/z* 275 which includes assignments of dimer products resulting from the reaction of primary products with Criegee intermediates. The *m/z* intensities will be a function of both analyte concentration and ionization efficiency; we relate relative intensity changes to relative concentration changes in the aerosol, but note that the most intense peaks are not necessarily the most abundant aerosol species. The peaks marked (*) are cut off on the expanded scale.

have been proposed in the literature, many of the proposed mechanisms are speculative and the kinetics essentially unknown. We proceeded by introducing simplifications to reduce parametric uncertainty in the model and align our mechanism with the main dimeric products observed in our EESI-MS and liquid chromatography (LC)-MS analysis (Figure 2b), and previous studies [*Zahardis et al*., 2005; *Reynolds et al*., 2006; *Lee et al*., 2012]. This assigned a single rate constant to all CI + carboxylic acid (k_b) and CI + aldehyde (k_c) reactions. Other reactions were omitted altogether. CI self-reactions, second order in [CI], were neglected due to the short CI lifetime and hence low steady state [CI]. The kinetics of CI + alkene reactions have not been studied experimentally, but the theoretical study of *Vereecken et al*. [2014] concluded that they are orders of magnitude slower than reactions with carboxylic acids and carbonyls for a given CI. However, we note the very recent study of *Wang et al*. [2016] and the earlier work of *Katrib et al*. [2004] which point to a potentially significant role for this reaction.

Omission of these potential CI sinks in the model may have led to overestimation of [CI] and hence underestimation of k_b and k_c which were varied to obtain a good fit to the measured data in the model. In addition, the missing CI + alkene reaction possibly underestimates the oleic acid loss rate. However, this simplified mechanism minimizes the parametric uncertainty associated with tuning the model rate constants to match the observations given the limited number of assigned products. We also believe that it is chemically sensible to lump the rate constants based on functional group reactivity.

3. Experimental Results and Discussion

3.1. Product Determination by Mass Spectrometry

A typical mass spectrum obtained from the EESI-MS analysis of oleic acid aerosol, partially oxidized with ozone, is given in Figure 3. The spectrum was acquired in negative ionization mode, meaning that functional groups which are readily deprotonated, such as carboxylic acids, are efficiently detected. Unreacted oleic acid was detected at *m/z* 281.2486. The peaks at *m/z* 157.1234, 171.1027, and 187.0976 were assigned as the three low volatility C_9 products from Figure 2: nonanoic acid (NA), 9-oxononanoic acid (9-ON), and azaleic acid (AA). The other C_9 product, nonanal (NN), is highly volatile and has been seen to partition into the gas phase [*Vesna et al*., 2009] causing evaporative size changes [*Dennis-Smither et al*., 2012]. In addition, its aldehyde functional group would not be readily ionized by deprotonation.

The Criegee intermediates CI-157 and CI-187 are isobaric with NA and AA, but we assume that, if detected, they do not make a significant contribution to the observed peak intensities due to their low concentrations. There is a small additional "monomer" peak at *m/z* 203.0925, also observed by *Reynolds et al*. [2006] which increases in intensity with ozone exposure and has a molecular formula consistent with a hydroperoxide product. This could form following decomposition of higher molecular weight products or reaction of the

Table 1. Species Detected Via Mass Spectrometry in Figures 3 and S1 Which Are Products of Ozonolysis Considered in the Model[a,b]

m/z	Name and Abbreviation	Possible Structures (Neutral)	Formation Reaction
157.1027	Nonanoic acid (NA)		CI-157 isomerization (k_a)
171.1027	9-Oxononanoic acid (9-ON)	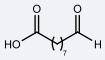	OA + O_3 (k_{OA+O3})
187.0976	Azaleic acid (AA)	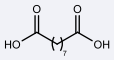	CI-187 isomerization (k_a)
281.2486	Oleic acid (OA)	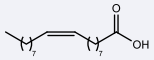	
329.2334	Dimer-329 (D-329)	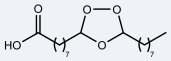	9-ON + CI-157 (k_c) (SOZ)
345.2283	Dimer-345 (D-345)	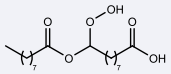	NA + CI-187 (k_b) (α-AAHP)
		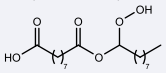	AA + CI-157 (k_b) (α-AAHP)
359.2075	Dimer-359 (D-359)	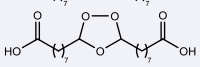	9-ON + CI-187 (k_c) (SOZ)
		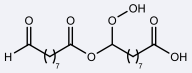	9-ON + CI-187 (k_b) (α-AAHP)
375.2024	Dimer-375 (D-375)	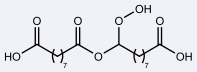	AA + CI-187 (k_b) (α-AAHP)

[a]Possible structures and the relevant formation reactions from Figure 2 are also listed.
[b]SOZ, secondary ozonide; α-AAHP, α-acyloxy alkyl hydroperoxide.

CIs with trace amounts of water. Other peaks in this region were not assigned and may be fragments or impurities from the electrospray solvent.

High molecular weight products are shown in the inset spectrum in Figure 3. The molecular formulae of the ions labelled "D" are consistent with dimers formed via CI-monomer reactions. Such products have been proposed in the literature and observed in previous studies [*Zahardis et al*., 2005; *Reynolds et al*., 2006; *Lee et al*., 2012]. Our mechanism includes formation of these products as given in Figure 2b. Specific possible structures for these species are given in Table S2. While the very recent study of *Wang et al*. [2016] proposes a route to high molecular weight products via CI + alkene reactions, the proposed C_{27} products were not identified in our measurements. The ions discussed here are listed in Table 1 for reference, along with potential structures and formation reactions.

Since LC-MS analysis involves separation and ionization of individual species according to retention time, it can be used to confirm that ions detected in direct infusion techniques correspond to stable molecular structures. LC-MS was applied here to oxidized oleic acid aerosol collected offline (described in the supporting information, Figure S1). Distinct LC-MS peaks were identified for *m/z* 375.2024 and *m/z* 359.2075. The time dependence of these dimer ions in EESI-MS was therefore compared to the model calculations alongside the monomers. Corresponding chemistry for D-329 and D-345 was also included in the model, but distinct LC-MS peaks could not be identified. Given the low abundance of these peaks in direct EESI-MS, it may be that they are lost in the LC-MS baseline or are not as stable during aerosol collection, storage, and extraction. The measured time dependence of *m/z* 329.2334 and 345.2283 was therefore not used to constrain the model performance.

3.2. Kinetics of Oleic Acid Loss

The kinetics of the heterogeneous reaction between oleic acid particles and ozone were monitored using EESI-MS. Relative particle-phase concentration changes were determined from relative intensity changes of reactant and product ions in the MS. The validity of this approach was demonstrated in *Gallimore and Kalberer* [2013] and is extended here to an ensemble of particles whose composition is changing as a function of time. Figure 4a shows the intensity of *m/z* 281.2486, assigned to deprotonated oleic acid $[OA–H]^-$, as a

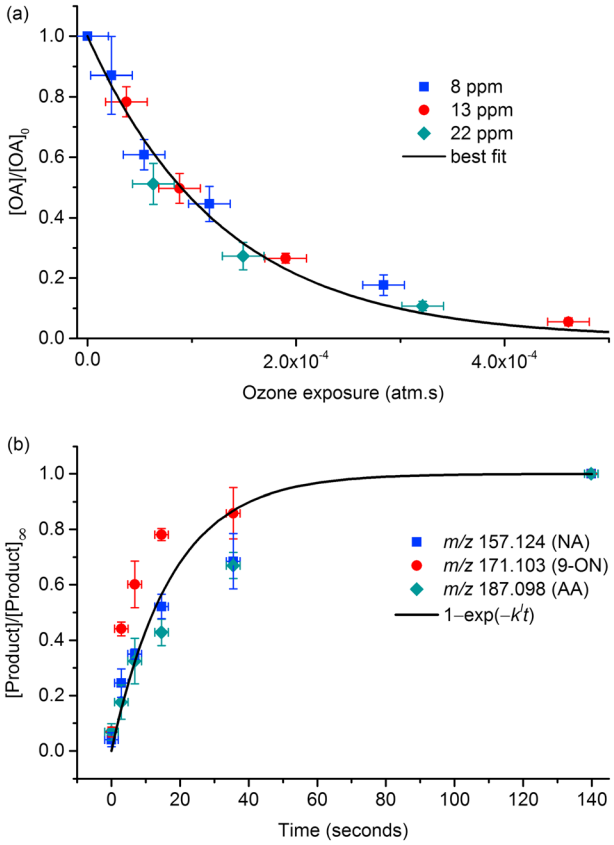

Figure 4. (a) Relative intensity of *m/z* 281.2486 ion corresponding to $[OA–H]^-$ as a function of ozone exposure ($P_{O3}.t$). On this scale, the data map well onto a single exponential best fit curve, suggesting that OA loss scales linearly with [O_3 (g)]. (b) Time series for 8 ppm ozone for ions assigned to primary C_9 products of oleic acid ozonolysis: nonanoic acid (NA), 9-oxononanoic acid (9-ON), and azaleic acid (AA). The ion intensities were scaled to their value at 140 s when essentially all of the oleic acid was depleted, and hence, the symbols for NA, 9-ON, and AA overlap at this time. The curve represents a hypothetical first-order production term from oleic acid; this describes NA and AA relatively well at short times but does not capture the behavior of 9-ON.

function of ozone exposure in the flow tube. The OA signal intensity is scaled relative to the spectrum of unreacted OA particles (i.e., before deliberate ozone exposure). Our data are all for conditions where only a small fraction of gas-phase ozone (<10%) is consumed by reactive uptake. Data from three different ozone concentrations are mapped onto a consistent ozone exposure ($P_{O3}.t$) scale; the individual time series are provided in the supporting information (Figure S2).

The consensus from previous particle-phase observations, based on the functional form and pronounced size dependence of OA loss, is that ozone reacts rapidly once accommodated onto oleic acid particles [*Morris et al*., 2002; *Smith et al*., 2002; *Hearn and Smith*, 2004; *Hearn et al*., 2005; *Ziemann*, 2005]. The exponential fit to all of our data in Figure 4a is consistent with the formulation of *Hearn et al*. [2005] for reaction in a surface film (case 3 kinetics):

$$\frac{[OA]}{[OA]_0} = \exp\left(-\frac{3\delta^2}{r}K_{H,O3}k^{II}P_{O3}t\right) \quad (1)$$

where δ is the thickness of the surface film, r is the particle radius, $K_{H,O3}$ is the Henry's law coefficient for ozone in oleic acid, k^{II} is the ozonolysis rate constant in the film, P_{O3} is the ozone partial pressure, and t is the reaction time. Our data from three different ozone concentrations are well described by a single fit to equation (1) in Figure 4a. Consistent with this formulation, our OA loss rate is a linear function of ozone concentration in the flow tube; we extracted pseudo first-order loss rates for each concentration from Figure 4a which are listed in Table S2. Previous data have been presented on an ozone exposure scale [*Morris et al*., 2002; *Hearn and Smith*, 2004], but to our knowledge this linearity in [O_3 (g)] has not been explicitly demonstrated before. We note that any possible secondary losses of oleic acid from other reactants such as Criegee intermediates do not perturb pseudo first-order OA losses and are therefore likely of minor importance.

The oleic acid loss measurements also enable us to derive a reactive uptake coefficient for ozone onto the aerosols. We follow the approach of *Hearn et al*. [2005] for reaction in a surface film and calculate $\gamma = 5\ (\pm 2) \times 10^{-4}$. This is relatively low compared to $\gamma \sim 8 \times 10^{-4}$ recommended by the review of *Zahardis and Petrucci* [2007] but is within the combined experimental uncertainty. This compares well to a recent determination by *Al-Kindi et al*. [2016], and lower values have been reported in other studies [*Dennis-Smither et al*., 2012].

3.3. Kinetics of Product Formation

EESI-MS allows us to monitor changes in a variety of products, including complex secondary species which are difficult to analyze using many alternative approaches. Now that we have established that

the oleic acid loss rate is first order in [O_3 (g)], we present the remaining data as a function of time rather than ozone exposure for more explicit comparison with PG-AM. We consider first the primary C_9 products, and Figure 4b shows measured time series for nonanoic acid (NA), 9-oxononanoic acid (9-ON), and azaleic acid (AA) for particles exposed to the lowest of the three ozone concentrations, 8 ppm. In this case ion intensities are scaled to a nominal final value when essentially all of the oleic acid had reacted.

These products are formed from the initial ozone-alkene reaction, either directly or via CI isomerization (Figure 2a). If we assume the particle-phase CI lifetime is short, we might therefore expect the products to all exhibit the same time dependence based on the characteristic time scale for oleic acid loss $k^I = 0.050\,s^{-1}$ from Table S2. The black curve in Figure 4b illustrates a calculated first-order production term alongside the measurements. We ascribe differences between the species, and deviation from this curve, to non–first-order processes, specifically oligomer formation reactions. The NA and AA data show a very similar time dependence which is close to the calculated curve over most of the reaction, although some differences can be seen at 40 s. This suggests that the loss processes for these species are relatively small. By contrast, the relative concentration of 9-ON deviates from this first-order behavior. We hypothesize that this is due to a bimolecular sink for 9-ON, such as reaction with CI:

$$\frac{d[\text{9-ON}]}{dt} = k_{\text{OA+O3}}[\text{OA}][\text{O}_3] - k_c[\text{9-ON}][\text{CI}] \tag{2}$$

The production term is unchanged from the black curve in Figure 4b and will be largest at the start of the reaction. However, the loss term will increase as 9-ON builds up. On a relative concentration scale, the net effect of this scenario is to make the product time series approach a maximum more rapidly, consistent with the observed 9-ON profile. We quantitatively assess the importance of this reaction and other particle-phase processes using an explicit numerical aerosol model in the following section.

4. Model Simulations of Experimental Observations

4.1. EESI-MS Data

To better understand the time dependence of our aerosol chemical composition measurements, we introduce a model which explicitly simulates the underlying processes relevant to organic aerosol aging, the Pretty Good Aerosol Model (PG-AM). This framework also allows us to investigate other observations such as the size-dependent reactivity of oleic acid particles [*Morris et al*., 2002; *Smith et al*., 2002] and particle volume changes as a consequence of ozone uptake and product evaporation [*Dennis-Smither et al*., 2012]. Figure 5 shows modeled time series for oleic acid and a range of primary and secondary products alongside the EESI-MS measurements. The oleic acid losses (Figure 5a) are captured well by the model using the literature parameters specified in Table S1. The accommodation coefficient α_{O3} is a poorly constrained parameter for this system, and $\alpha_{O3} = 10^{-3}$ was found to give a good fit to the data in Figure 5a and for the higher ozone concentrations (Figure S3).

The model shows a strong radial gradient in [O_3 (l)] during the simulation (Figure S4) which is consistent with the picture of rapid ozone reaction following accommodation to the particle. As a consequence, the modeled oleic acid loss rate exhibits a profound particle size dependence. We characterized the competition between ozone diffusion through the particle and reaction with an oleic acid molecule in terms of a reacto-diffusive length, $l = D_{O3}/k_{O3+OA}[\text{OA}]$. For $r_{\text{eff}} = 250$ nm used here, we obtained $l < 8$ nm for the early part of the reaction, indicating that the ozone remains confined to the outer few percent of the particle until most of the oleic acid is consumed. This agrees well with an experimental estimate of reacto-diffusive length of 10 nm [*Morris et al*., 2002]. The oleic acid, meanwhile, shows only small gradients due to rapid bulk diffusion, in agreement with the modeling study of *Shiraiwa et al*. [2010] and consistent with particles remaining liquid throughout ozonolysis [*Hosny et al*., 2016].

We also simulated product formation and secondary chemistry occurring in the particles. Since the rates of oligomer formation reactions are not at all known, we proceeded by fixing $k_a = 500\,s^{-1}$ based on *Welz et al*. [2012] and varying the oligomerization reaction rates (k_b and k_c) to obtain the best fit to the MS data. We found that the model was not sensitive to the absolute magnitude of k_a, provided $k_a >> k^I$.

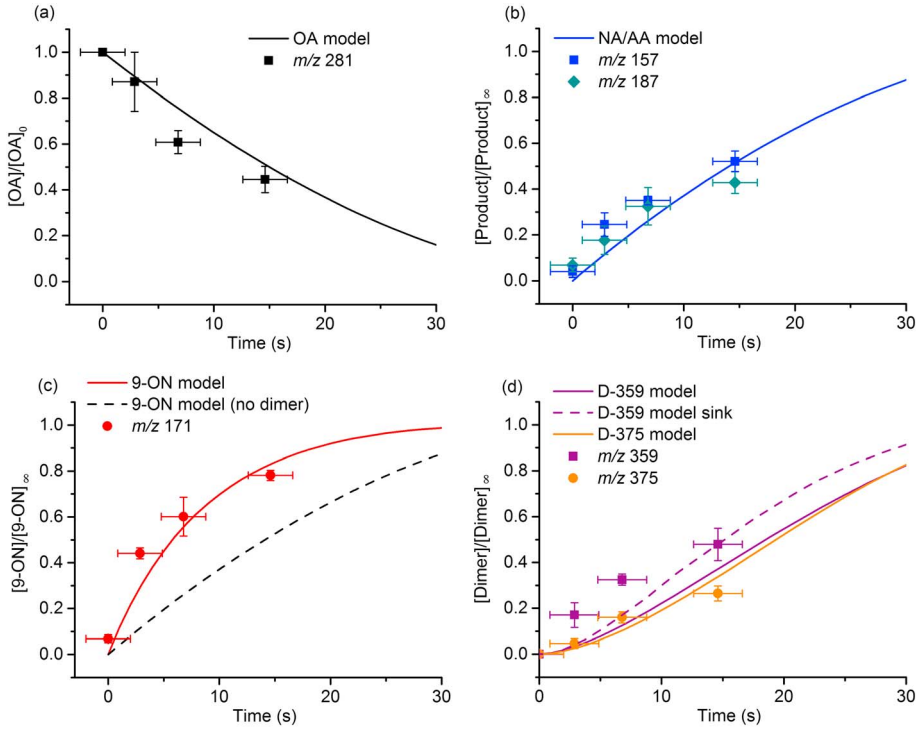

Figure 5. Modeled concentrations as a function of time for (a) oleic acid (OA), (b) nonanoic acid (NA) and azaleic acid (AA), (c) 9-oxononanoic acid (9-ON), and (d) dimer products, D-359 and D-375. EESI-MS measurements with 8 ppm ozone are included as discrete points, and both model and experimental results are scaled to aid comparison. The model shows a close fit to the measured OA (Figure 5a) and primary product (Figures 5b and 5c) data, and reasonable agreement for the dimer products (Figure 5d). NA and AA (Figure 5b) have the same modeled time dependence owing to the symmetry of the mechanism (Figure 2). The dashed line in Figure 5c represents a simulation with the dimer chemistry switched off, and the dashed line in Figure 5d includes a unimolecular sink for D-359 ($k_{sink} = 0.01\ s^{-1}$) as a proxy for further dimer reactions.

Agreement between the modeled and measured concentrations was found for all of the product species (Figures 5b–5d), given the experimental and parametric uncertainty involved in this comparison. In particular, the characteristic difference in the 9-ON time series compared to the other primary products noted in Figure 4b was reproduced by including the oligomerization reactions described in Figure 2b.

9-oxononanoic acid contains an aldehyde functional group as well as the acid group also present in azaleic acid and nonanoic acid. We therefore found the predominant reaction of 9-ON with Criegee intermediates to be via the aldehyde group (k_c), with a relatively lower rate of CI-acid reaction (k_b) for all three C_9 products. The dashed line in Figure 5c shows the simulated 9-ON profile with oligomerization switched off, a demonstrably poorer agreement. The products of CI-aldehyde reactions are secondary ozonides (SOZs), and our results are consistent with evidence from the solution-phase literature that SOZs form in high yields [*Geletneky and Berger*, 1998; *Carey and Sundberg*, 2008]. However, they contrast with the findings of *Mochida et al.* [2006] who reported that the highest dimer yields from oleic acid ozonolysis result from CI-acid reactions.

Since the model is not sensitive to the absolute magnitude of k_a, the relative rates k_b/k_a and k_c/k_a determine the fate of the CIs in the particle, specifically the branching between isomerization and oligomerization. We found $k_b/k_a = 0.3\ M^{-1}$ and $k_c/k_a = 2\ M^{-1}$, respectively, gave good fits to the primary product time series (Figures 5b and 5c).

Figure 5d shows the modeled dimer concentrations, which show reasonable agreement with the experimental values. We found that the modeled profiles were only weakly sensitive to the relative rates k_b/k_a and k_c/k_a, and so we used the primary product time series to constrain these ratios. The simulated D-359 profile is initially too low, possibly as a consequence of missing reactions which consume the dimer. The dashed line in Figure 5d shows a model run with a pseudo first-order dimer loss included ($k_{sink} = 0.01\ s^{-1}$) as a proxy for

Table 2. Summary of Experimental Studies of Oleic Acid Aerosol Ozonolysis Containing Explicit Time Series for Oleic Acid Loss[a,b]

Study	Particle Radius (nm)	$[O_3]$ (ppm)	Model Parameters	Experimental
This work	~250	8–22	Base case (Table S1)	Aerosol ensemble from nebulizer (ethanol solution); flow tube; EESI-MS
Ziemann [2005]	~200	2.8	$\alpha_{O3} = 2 \times 10^{-3}$	Aerosol ensemble by homogeneous nucleation; smog chamber; TDPBMS
Hearn and Smith [2004]	~400	100	$\alpha_{O3} = 1.5 \times 10^{-3}$	Aerosol ensemble from nebulizer (pure OA); flow tube; aerosol CIMS
Dennis-Smither et al. [2012]	4580 (core shell*)	6	$\alpha_{O3} = 5 \times 10^{-4}$	OA coagulation with single NaCl core*; optical tweezers; Raman and Mie scattering

[a]The measurements were compared to model simulations under the same conditions, and the best agreement was obtained by adjusting the accommodation coefficient for ozone, α_{O3}, as a proxy for experimental and parametric uncertainty.
[b]TDPBMS, thermal desorption particle beam mass spectrometer; CIMS, chemical ionization mass spectrometer.
*The particles consisted of a liquid oleic acid droplet of the specified total radius, containing an unreactive sodium chloride inclusion of approximately 2 μm radius (spherically equivalent size).

possible further decomposition or oligomerization reactions. This improves the agreement for D-359 in an analogous manner to 9-ON, but the nature of this removal could not be reliably identified from the observed products.

4.2. Simulation of Other Experimental Data

A number of previous studies have presented measurements amenable to process modeling. We focus on three experimental studies which present explicit time-dependent measurements of oleic acid concentration changes [*Hearn and Smith*, 2004; *Ziemann*, 2005; *Dennis-Smither et al*., 2012]. These studies span a range of particle sizes, reaction times, and ozone concentrations and so present a test of the model performance. The studies are summarized in Table 2. In each case, the model parameters were as used as presented in Table S1, while α_{O3} was adjusted to obtain a good fit to the oleic acid loss measurements.

In general, the model does well in reproducing these observations over a range of particle sizes (~200–5000 nm) and oxidation time scales (seconds to tens of minutes) using the same diffusion and reaction parameters as before. Figure 6a shows oleic acid loss data for the *Dennis-Smither et al*. [2012] study, for a single micron-sized particle. We were able to reproduce other studies to a similarly high degree of agreement, and the time series for *Hearn and Smith* [2004] and *Ziemann* [2005] are presented in Figures 6b and 6c, respectively. We feel that close model agreement with a range of measurements helps to rationalize previous observations and provide a more coherent picture of the ozonolysis of oleic acid particles with respect to relevant physicochemical parameters (Table S1).

The modified α_{O3} values can be seen as a reflection of the variation of measured loss rates: For instance, *Dennis-Smither et al*. [2012] note that their oleic acid loss is slower relative to the submicron particle studies. Nevertheless, α_{O3} was only varied by ± 50% to obtain good agreement across this range of measurements, consistent with the experimental uncertainty on such determinations which is usually high. The more significant reduction in α_{O3} for the case of *Dennis-Smither et al*. [2012] may also be the result of the different experimental approaches. Our composition measurements involve sampling a steady state ozone-exposed aerosol ensemble from a flow tube, while the static chamber setup used in the single particle study may have required a nonnegligible gas-phase equilibration time, leading to lower and uncertain ozone concentrations early in the reaction. We also note the different methods of aerosol preparation: in our case, we prepared the aerosol from an OA solution using a nebulizer, while in *Dennis-Smither et al*. [2012] the aerosol was prepared from the coagulation of homogeneously nucleated OA particles with a sodium chloride "core" particle in the optical trap. Given the combined experimental uncertainty, and possible systematic differences in particle properties, we consider the agreement is very encouraging.

In addition to oleic acid loss from particles, we investigated the particle evaporation behavior presented in *Dennis-Smither et al*. [2012] using PG-AM. The same chemical scheme as Figure 2 was used again here, and gas-particle partitioning coefficients for oleic acid and each of the C_9 products were calculated according to their saturation vapor pressures (Table S1). Dimer products were assumed to be nonvolatile.

The model captures the observed size changes over both short and long time scales. The small initial increase in volume (Figure 6d), corresponding to only a few nanometers in radius, is explained in the model by the formation of volatile products, particularly nonanal, whose initial evaporation rate from the particle is

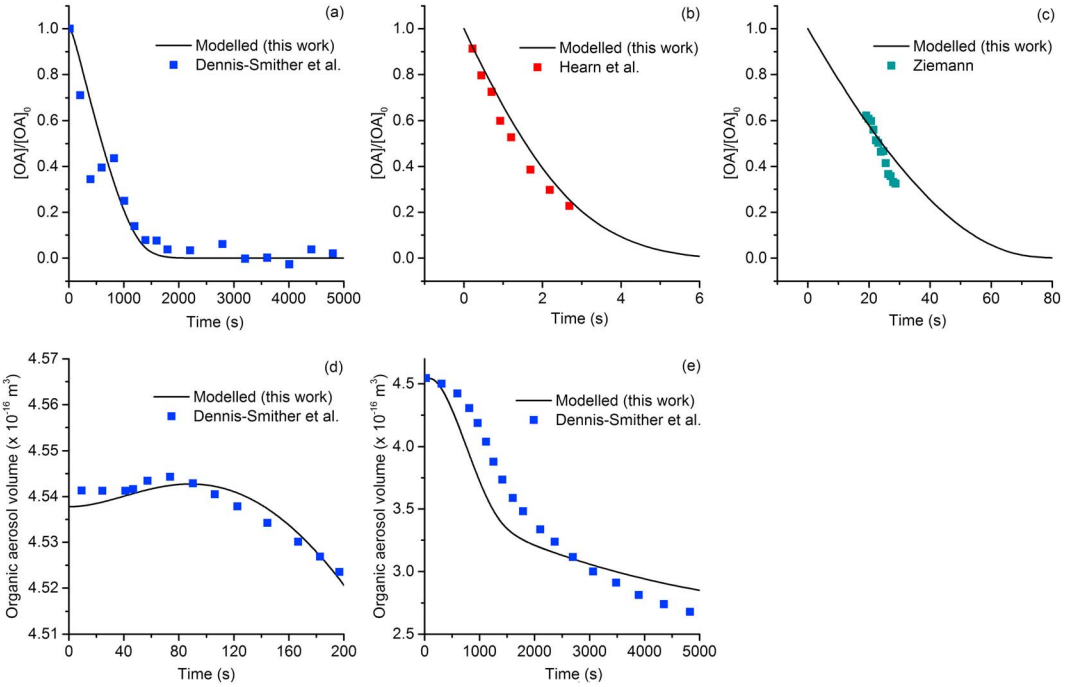

Figure 6. Model simulations compared with observations of oleic acid loss for (a) *Dennis-Smither et al.* [2012], (b) *Hearn and Smith* [2004], and (c) *Ziemann* [2005]. We also simulate the single particle volume change of *Dennis-Smither et al.* [2012] (d) at the start of ozonolysis and (e) over the experiment time scale. The model parameters were as for the base case (Table S1) with changes according to the experiment-specific parameters in Table 2. For the simulation in Figure 6b, precision and accuracy checks were turned off from Mathematica's NDSolve routine to allow the model to execute. The experimental data in Figure 6c were obtained directly from P. Ziemann since the figure presented in *Ziemann* [2005] contains a small error in the oleic acid time axis. These data were offset in time to coincide with the simulated curve and account for the mixing period in the chamber experiment.

lower than its production rate. The consequence is an initial buildup of particle-phase nonanal followed by evaporation on longer time scales (Figure 6e).

The relatively slow initial evaporation of nonanal, despite its high vapor pressure, would be reconciled by a small accommodation coefficient for nonanal and hence slow transfer out of the particle. $\alpha_{org} = 10^{-5}$ was used in the model, which also leads to the gradual evaporation of nonanoic acid and 9-oxononanoic acid on long time scales after the OA was consumed. This is consistent with the hypothesis of *Dennis-Smither et al.* [2012] for their continuing particle volume loss. Slow evaporation behavior may also be a consequence of changes in diffusion within the particle which are not considered in the model. *Hosny et al.* [2016] observed the viscosity of oleic acid aerosol increased during ozonolysis, while *Lee et al.* [2012] hypothesized an amorphous "crust" formed on the surface of arachidonic acid during ozonolysis, which like oleic acid is an unsaturated, hydrophobic acid. *Dennis-Smither et al.* [2012] observed a longtime increase in the apparent refractive index retrieved from the evaporating droplet, assuming the particle was homogeneous, even after the size had reached a steady value. This was considered to indicate the possible slow relaxation in a concentration gradient within the particle or a restructuring in particle morphology.

The magnitude of the modeled and measured evaporative losses is comparable over the course of the reaction (Figure 6e). However, there is an overprediction of evaporation at short times and slight underprediction at longer times. The model chemical scheme favors formation of nonanal and azaleic acid from the initial cycloaddition reaction; adjusting this branching ratio closer to 1:1 to favor more (semivolatile) nonanoic acid and 9-oxononanoic acid production would reconcile these differences.

We revisit the ozonolysis mechanism to interpret some of the kinetic parameters derived from this model analysis. Decomposition of the unstable primary ozonide (Figure 2a) forms the initial functional groups (CI and aldehyde) in close proximity and oriented toward each other, which may promote transient intermolecular interaction between the products. Furthermore, previous studies have noted that the surrounding

fatty acid medium is likely to be ordered into a rod-like arrangement of molecules [*Iwahashi et al*., 2000] owing to the propensity for oleic acid to form hydrogen-bonded acid pairs. These geometric constraints may lead to formation of a "caged" CI-aldehyde complex.

In such a scenario, the CI encounters a high effective aldehyde concentration immediately, whereas other bimolecular reactions require CI reorientation and diffusion. This is a plausible explanation for the much larger 9-ON sink (k_c) than for the other C_9 products (k_b). However, CI escape must occur to some extent, to explain the latter hydroperoxide products and also secondary ozonides produced by cross reactions from two ozonolysis events, such as *m/z* 359.

The slow evaporation of nonanal, represented in the model by a small mass accommodation coefficient, could also be a consequence of restricted escape from such a "caged" geometry. Using a larger value for accommodation ($\alpha_{nonanal} \sim 0.1$) would require a lifetime for the complex on the order of tens of seconds to explain the evaporation data. This would appear to be long for a transient complex, possibly suggesting a role for decomposition of initial products (such as oligomers) to yield nonanal, as hinted at by the dimer "sink" reaction discussed in Figure 5d. Ultimately, however, the available data do not permit us to distinguish between these hypotheses.

4.3. Comparison With Other Modeling Studies

Utilizing a detailed model can provide insight into aerosol processes as demonstrated in the sections above. However, it is important to recognize that the model requires appropriate and physically realistic constraints, specifically in terms of the input parameters used to represent reaction, diffusion, and interfacial transport. Our preference is to fix as many of the parameters as possible based on literature values, either from experiment or theory. Fortunately, for the oleic acid-ozone system, a relatively large quantity of relevant parametric data is available and consequently few parameters were optimized by comparison with experimental data. We find that the parameters reported in Table S1 can adequately describe experimental observations within combined experimental and parametric uncertainties.

Similar "fixed parameter" case studies have also proven successful in detailed modeling by *Shiraiwa et al*. [2010] and *Houle et al*. [2015] for heterogeneous aging of organic aerosols. An alternative approach which samples more of the model parameter space by globally optimizing parameter sets with respect to experimental aerosol measurements has been reported recently [*Berkemeier et al*., 2016]. This approach may be particularly useful if important parameters are not readily available from the literature for the system of interest. *Berkemeier et al*. [2016] point out that large experimental data sets are required to adequately constrain degrees of freedom in the model, but we note that even for a relatively well studied system such as the reactive uptake of ozone to oleic acid particles, appreciable differences in key parameters such as k_{OA+O3} can arise ($k_{PG\text{-}AM}/k_{Hosny} \sim 1500$) [*Hosny et al*., 2016]. Both approaches may help to assess and constrain relevant physicochemical aerosol parameters in the future.

5. Conclusions

The combination of measurement and modeling presented in this study represents an important step forward in the detailed understanding of organic aerosol processes, especially for systems such as the ozonolysis of oleic acid aerosol where competition between transport and reaction determines the time scale for atmospheric processing.

The ability of EESI-MS to make aerosol kinetics measurements on a molecular level has been demonstrated for the first time using the ozonolysis of oleic acid aerosol as a model system. Useful quantitative information could be derived from the relative intensities of $[M–H]^-$ reactant and product ions in the EESI mass spectra.

A process-level model was used to interpret these measurements and complementary observations from previous studies. Differences in the measured appearance rates of ozonolysis products were used to constrain the relative rates of secondary reactions in the particles. We concluded that the lifetime of Criegee intermediates in the particle was short with respect to isomerization, but that a significant sink for CIs may involve secondary ozonide formation through reaction with the aldehyde group of 9-ON. The reaction between oleic acid and ozone was found to occur in a near-surface layer, in good agreement with experimental studies.

Model performance was further assessed by comparison to other studies with large differences in time scales, ozone concentrations, and particle sizes. Chemical and evaporative changes were both reproduced well. Significantly, the chemical insight provided by the new product measurements was used to construct a model chemical mechanism able to successfully explain independent measurements of the evolving particle size. Comparing to multiple experimental observables both improves confidence in the model performance and strengthens the conclusions of experimental work.

The difficulty of interrogating the kinetics of reactive intermediates in particles was demonstrated in this study. This represents an ongoing challenge for the organic aerosol community. Including a mechanism for CI reactions in the model allowed relative rates (e.g., k_c/k_a) to be assessed and represents a useful starting point. However, since the rate-determining step for product formation was the initial ozone-alkene cycloaddition, absolute rates of CI reactions could not be determined. In addition, there are inherent limits to process modeling based on the unavailability or uncertainty of relevant physical parameters for the system under study. Nevertheless, our methodology provides insight into the kinetic regimes and chemical changes associated with organic aerosol aging, and these issues will be addressed in future studies.

Acknowledgments
This work was supported by the UK Natural Environment Research Council (NERC grant NE/I528277/1) and the European Research Council (ERC starting grant 279405 and the Atmospheric Chemistry Climate Interactions (ACCI) project, grant 267760). PTG thanks NCAS Climate for support. We thank the reviewers for insightful and constructive feedback on the manuscript. Data may be obtained from the University of Cambridge Data Repository at https://doi.org/10.17863/CAM.7996.

References

Al-Kindi, S., F. D. Pope, D. C. Beddows, W. J. Bloss, and R. M. Harrison (2016), Size dependent chemical ageing of oleic acid aerosol under dry and humidified conditions, *Atmos. Chem. Phys.*, *16*, 15,561–15,579, doi:10.5194/acp-16-15561-2016.

Barsanti, K. C., and J. F. Pankow (2005), Thermodynamics of the formation of atmospheric organic particulate matter by accretion reactions—2. Dialdehydes, methylglyoxal, and diketones, *Atmos. Environ.*, *39*(35), 6597–6607, doi:10.1016/j.atmosenv.2005.07.056.

Barsanti, K. C., and J. F. Pankow (2006), Thermodynamics of the formation of atmospheric organic particulate matter by accretion reactions-Part 3: Carboxylic and dicarboxylic acids, *Atmos. Environ.*, *40*(34), 6676–6686, doi:10.1016/j.atmosenv.2006.03.013.

Berkemeier, T., A. J. Huisman, M. Ammann, M. Shiraiwa, T. Koop, and U. Pöschl (2013), Kinetic regimes and heterogeneous reactions in atmospheric aerosols and clouds: A general classification scheme, *Atmos. Chem. Phys.*, *13*, 6663–6686, doi:10.5194/acp-13-6663-2013.

Berkemeier, T., S. S. Steimer, U. K. Krieger, T. Peter, U. Pöschl, M. Ammann, and M. Shiraiwa (2016), Ozone uptake on glassy, semi-solid and liquid organic matter and the role of reactive oxygen intermediates in atmospheric aerosol chemistry, *Phys. Chem. Chem. Phys.*, *18*(18), 12,662–12,674, doi:10.1039/C6CP00634E.

Boucher, O., et al. (2013), Clouds and Aerosols, in *Climate Change 2013: The Physical Science Basis. Contribution of Working Group I to the Fifth Assessment Report of the Intergovernmental Panel on Climate Change*, edited by T. F. Stocker et al., Cambridge Univ. Press, Cambridge, U. K., and New York.

Carey, F. A., and R. J. Sundberg (2008), *Advanced Organic Chemistry*, 5th ed., Springer, New York.

Dennis-Smither, B. J., R. E. H. Miles, and J. P. Reid (2012), Oxidative aging of mixed oleic acid/sodium chloride aerosol particles, *J. Geophys. Res.*, *117*, D20204, doi:10.1029/2012JD018163.

Gallimore, P. J., and M. Kalberer (2013), Characterizing an extractive electrospray ionization (EESI) source for the online mass spectrometry analysis of organic aerosols, *Environ. Sci. Technol.*, *47*(13), 7324–31, doi:10.1021/es305199h.

Geletneky, C., and S. Berger (1998), The mechanism of ozonolysis revisited by 17O-NMR spectroscopy, *Eur. J. Org. Chem.*, *1998*(8), 1625–1627, doi:10.1002/(SICI)1099-0690(199808)1998:8<1625::AID-EJOC1625>3.0.CO;2-L.

Griffiths, P. T., C. L. Badger, R. A. Cox, M. Folkers, H. H. Henk, and T. F. Mentel (2009), Reactive uptake of N_2O_5 by aerosols containing dicarboxylic acids. Effect of particle phase, composition, and nitrate content, *J. Phys. Chem. A*, *113*(17), 5082–5090, doi:10.1021/jp8096814.

Hearn, J. D., and G. D. Smith (2004), Kinetics and product studies for ozonolysis reactions of organic particles using aerosol CIMS, *J. Phys. Chem. A*, *108*(45), 10,019–10,029, doi:10.1021/jp0404145.

Hearn, J. D., A. J. Lovett, and G. D. Smith (2005), Ozonolysis of oleic acid particles: evidence for a surface reaction and secondary reactions involving Criegee intermediates, *Phys. Chem. Chem. Phys.*, *7*(3), 501–11.

Hosny, N. A., et al. (2016), Direct imaging of changes in aerosol particle viscosity upon hydration and chemical aging, *Chem. Sci.*, *7*, 1357–1367, doi:10.1039/C5SC02959G.

Houle, F. A., W. D. Hinsberg, and K. R. Wilson (2015), Oxidation of a model alkane aerosol by OH radical: The emergent nature of reactive uptake, *Phys. Chem. Chem. Phys.*, *17*(6), 4412–4423, doi:10.1039/c4cp05093b.

Iwahashi, M., Y. Kasahara, H. Matsuzawa, K. Yagi, K. Nomura, H. Terauchi, Y. Ozaki, and M. Suzuki (2000), Self-diffusion, dynamical molecular conformation, and liquid structures of n-saturated and unsaturated fatty acids, *J. Phys. Chem. B*, *104*, 6186–6194.

Katrib, Y., S. T. Martin, H.-M. Hung, Y. Rudich, H. Zhang, J. G. Slowik, P. Davidovits, J. T. Jayne, and D. R. Worsnop (2004), Products and mechanisms of ozone reactions with oleic acid for aerosol particles having core-shell morphologies, *J. Phys. Chem. A*, *108*, 6686–6695.

Keyser, L. F. (1984), High-pressure flow kinetics. A study of the OH + HCl reaction from 2 to 100 Torr, *J. Phys. Chem.*, *88*(20), 4750–4758.

Kroll, J. H., and J. H. Seinfeld (2008), Chemistry of secondary organic aerosol: Formation and evolution of low-volatility organics in the atmosphere, *Atmos. Environ.*, *42*(16), 3593–3624, doi:10.1016/j.atmosenv.2008.01.003.

Lee, J. W. L., V. Carrascón, P. J. Gallimore, S. J. Fuller, A. Björkegren, D. R. Spring, F. D. Pope, and M. Kalberer (2012), The effect of humidity on the ozonolysis of unsaturated compounds in aerosol particles, *Phys. Chem. Chem. Phys.*, *14*(22), 8023–31, doi:10.1039/c2cp24094g.

Liggio, J., and S. M. Li (2006), Reactive uptake of pinonaldehyde on acidic aerosols, *J. Geophys. Res.*, *111*, D24303, doi:10.1029/2005JD006978.

McNeill, V. F., J. L. Woo, D. D. Kim, A. N. Schwier, N. J. Wannell, A. J. Sumner, and J. M. Barakat (2012), Aqueous-phase secondary organic aerosol and organosulfate formation in atmospheric aerosols: A modeling study, *Environ. Sci. Technol.*, *46*, 8075–8081, doi:10.1021/es3002986.

Mochida, M., K. Yasuyuki, K. Kawamura, Y. Nojiri, and K. Suzuki (2002), Fatty acids in the marine atmosphere: Factors governing their concentrations and evaluation of organic films on sea-salt particles, *J. Geophys. Res.*, *107*(D17), 4325, doi:10.1029/2001JD001278.

Mochida, M., Y. Katrib, J. T. Jayne, D. R. Worsnop, and S. T. Martin (2006), The relative importance of competing pathways for the formation of high-molecular-weight peroxides in the ozonolysis of organic aerosol particles, *Atmos. Chem. Phys.*, *6*, 4851–4866, doi:10.5194/acp-6-4851-2006.

Morris, J. W., P. Davidovits, J. T. Jayne, J. L. Jimenez, Q. Shi, C. E. Kolb, and D. R. Worsnop (2002), Kinetics of submicron oleic acid aerosols with ozone: A novel aerosol mass spectrometric technique, *Geophys. Res. Lett.*, *29*(9), 3–6, doi:10.1029/2002GL014692.

Murphy, D. M., D. J. Cziczo, K. D. Froyd, P. K. Hudson, B. M. Matthew, A. M. Middlebrook, R. E. Peltier, A. Sullivan, D. S. Thomson, and R. J. Weber (2006), Single-particle mass spectrometry of tropospheric aerosol particles, *J. Geophys. Res.*, *111*, D23S32, doi:10.1029/2006JD007340.

Noziere, B., et al. (2015), The molecular identification of organic compounds in the atmosphere: State of the art and challenges, *Chem. Rev.*, *115*(10), 3919–3983, doi:10.1021/cr5003485.

Pope, C. A., M. Ezzati, and D. W. Dockery (2009), Fine-particulate air pollution and life expectancy in the United States, *N. Engl. J. Med.*, *360*(4), 376–86, doi:10.1056/NEJMsa0805646.

Reynolds, J. C., D. J. Last, M. McGillen, A. Nijs, A. B. Horn, C. Percival, L. J. Carpenter, and A. C. Lewis (2006), Structural analysis of oligomeric molecules formed from the reaction products of oleic acid ozonolysis, *Environ. Sci. Technol.*, *40*(21), 6674–6681, doi:10.1021/es060942p.

Robinson, A. L., N. M. Donahue, M. K. Shrivastava, E. A. Weitkamp, A. M. Sage, A. P. Grieshop, T. E. Lane, J. R. Pierce, and S. N. Pandis (2007), Rethinking organic aerosols: Semivolatile emissions and photochemical aging, *Science*, *315*(80), 1259–1262, doi:10.1126/science.1133061.

Rogge, W. F., L. M. Hildemann, M. A. Mazurek, G. R. Cass, and B. R. T. Simonelt (1993), Sources of fine organic aerosol. 2. Noncatalyst and catalyst-equipped automobiles and heavy-duty diesel trucks, *Environ. Sci. Technol.*, *27*, 636–651.

Rudich, Y., N. M. Donahue, and T. F. Mentel (2007), Aging of organic aerosol: Bridging the gap between laboratory and field studies, *Annu. Rev. Phys. Chem.*, *58*, 321–352, doi:10.1146/annurev.physchem.58.032806.104432.

Shiraiwa, M., C. Pfrang, and U. Pöschl (2010), Kinetic multi-layer model of aerosol surface and bulk chemistry (KM-SUB): The influence of interfacial transport and bulk diffusion on the oxidation of oleic acid, *Atmos. Chem. Phys.*, *10*(1), 281–326, doi:10.5194/acp-10-3673-2010.

Smith, G. D., E. Woods, C. L. DeForest, T. Baer, and R. E. Miller (2002), Reactive uptake of ozone by oleic acid aerosol particles: Application of single-particle mass spectrometry to heterogeneous reaction kinetics, *J. Phys. Chem. A*, *106*(35), 8085–8095, doi:10.1021/jp020527t.

Stewart, D. J., P. T. Griffiths, and R. A. Cox (2004), Reactive uptake coefficients for heterogeneous reaction of N_2O_5 with submicron aerosols of NaCl and natural sea salt, *Atmos. Chem. Phys.*, *4*(2), 1381–1388, doi:10.5194/acpd-4-569-2004.

Vereecken, L., H. Harder, and A. Novelli (2014), The reactions of Criegee intermediates with alkenes, ozone, and carbonyl oxides, *Phys. Chem. Chem. Phys.*, *16*(9), 4039–49, doi:10.1039/c3cp54514h.

Vesna, O., M. Sax, M. Kalberer, A. Gaschen, and M. Ammann (2009), Product study of oleic acid ozonolysis as function of humidity, *Atmos. Environ.*, *43*(24), 3662–3669, doi:10.1016/j.atmosenv.2009.04.047.

Wang, G., K. Kawamura, S. Lee, K. Ho, and J. Cao (2006), Molecular, seasonal, and spatial distributions of organic aerosols from fourteen Chinese cities, *Environ. Sci. Technol.*, *40*(15), 4619–4625, doi:10.1021/es060291x.

Wang, M., L. Yao, J. Zheng, X. Wang, J. Chen, X. Yang, D. R. Worsnop, N. M. Donahue, and L. Wang (2016), Reactions of atmospheric particulate stabilized Criegee intermediates lead to high-molecular-weight aerosol components, *Environ. Sci. Technol.*, *50*(11), 5702–5710, doi:10.1021/acs.est.6b02114.

Welz, O., J. D. Savee, D. L. Osborn, S. S. Vasu, C. J. Percival, D. E. Shallcross, and C. A. Taatjes (2012), Direct kinetic measurements of Criegee intermediate (CH_2OO) formed by reaction of CH_2I with O_2, *Science*, *335*(80), 204–207, doi:10.1126/science.1213229.

Zahardis, J., and G. A. Petrucci (2007), The oleic acid-ozone heterogeneous reaction system: Products, kinetics, secondary chemistry, and atmospheric implications of a model system—A review, *Atmos. Chem. Phys.*, *7*(5), 1237–1274, doi:10.5194/acp-7-1237-2007.

Zahardis, J., B. W. LaFranchi, and G. A. Petrucci (2005), Photoelectron resonance capture ionization-aerosol mass spectrometry of the ozonolysis products of oleic acid particles: Direct measure of higher molecular weight oxygenates, *J. Geophys. Res.*, *110*, D08307, doi:10.1029/2004JD005336.

Zhao, R., E. L. Mungall, A. K. Y. Lee, D. Aljawhary, and J. P. D. Abbatt (2014), Aqueous-phase photooxidation of levoglucosan—A mechanistic study using Aerosol Time of Flight Chemical Ionization Mass Spectrometry (Aerosol-ToF-CIMS), *Atmos. Chem. Phys.*, *14*, 9695–9706, doi:10.5194/acp-14-9695-2014.

Ziemann, P. J. (2005), Aerosol products, mechanisms, and kinetics of heterogeneous reactions of ozone with oleic acid in pure and mixed particles, *Faraday Discuss.*, *130*, 469–490, doi:10.1039/b417502f.

Ziemann, P. J., and R. Atkinson (2012), Kinetics, products, and mechanisms of secondary organic aerosol formation, *Chem. Soc. Rev.*, *41*(19), 6582–605, doi:10.1039/c2cs35122f.